JPET Fast Forward. Published on May 17, 2007 as DOI: 10.1124/jpet.107.121798
This article has not been copyedited and formatted. The final version may differ from this version.

Title page

Benzodiazepine Withdrawal-Induced Glutamatergic Plasticity Involves Upregulation of GluR1-Containing AMPA Receptors in Hippocampal CA1 Neurons

Jun Song, Guofu Shen, L. John Greenfield, Jr. and Elizabeth I. Tietz

Department of Physiology and Pharmacology (JS, GS, LJG, EIT), Department of Neurology (LJG), and the Cellular and Molecular Neurobiology Program (JS, GS, LJG, EIT), University of Toledo College of Medicine, Toledo, OH 43614

Running title page

Running title: Benzodiazepine Withdrawal-Induced AMPA Receptor Regulation

Corresponding Author:
Elizabeth I. Tietz, Ph.D.
Department of Physiology and Pharmacology
University of Toledo College of Medicine
Health Science Campus
(Formerly Medical University of Ohio)
3000 Arlington Ave., Mailstop 1008
Toledo, OH 43614
Tel: (419)383-4170
Fax: (419)383-2871
E-mail: liz.tietz@utoledo.edu

Text pages: 49
Tables: 2
Figures: 6
References: 40
Abstract: 251 words
Introduction: 645 words
Discussion: 2082 words

ABBREVATIONS: AMPA, alpha-Amino-3-hydroxy-5-methylisoxazole-4-propionic acid; GABA, gamma-amino butyric acid type A; NMDA, N-methyl-D-aspartate; CON, control; FZP, flurazepam; AKAP, A kinase-anchoring protein; PKA, cAMP-dependent protein kinase A; CaMKII, Ca^{2+}/calmodulin dependent protein kinase II; LTP, long-term potentiation; KA, kainate; NAS, 1-naphthylacetyl spermine; APV, DL-2-amino-5-phosphopentanoic acid; TTX, tetrodotoxin; RMP, Resting membrane potential; PDZ, PSD-95, Dlg and ZO-1; mEPSCs, miniature excitatory postsynaptic currents; GluR, glutamate receptor; so, stratum oriens; sp, stratum pyramidale; sr, stratum radiatum; PSD, postsynaptic density.

Recommended Section: Neuropharmacology

JPET Fast Forward. Published on May 17, 2007 as DOI: 10.1124/jpet.107.121798
This article has not been copyedited and formatted. The final version may differ from this version.

Abstract

Modification of glutamatergic synaptic function, a mechanism central to neuronal plasticity, may also mediate long-term drug effects, including dependence and addiction. Benzodiazepine withdrawal results in increased glutamatergic strength, but whether AMPARs are functionally and structurally remodeled during benzodiazepine withdrawal is uncertain. Whole-cell recordings of rat hippocampal CA1 neurons, either acutely-dissociated or in hippocampal slices, revealed that AMPAR function was enhanced up to 50% during flurazepam (FZP) withdrawal, without changes in whole-cell channel kinetic properties. Agonist-elicited AMPA currents showed a negative shift in rectification in the presence of spermine, suggesting augmented membrane incorporation of GluR2-lacking AMPARs. As GluR1-containing AMPARs are critical for activity-dependent alterations in excitatory strength, we sought to determine whether changes in GluR1 subunit distribution in CA1 neurons occurred during benzodiazepine withdrawal. Confocal image analysis revealed that FZP withdrawal promoted GluR1 subunit incorporation into somatic and proximal dendritic membranes of CA1 neurons, without GluR2 subunit alterations. Findings of immunoblot studies were consistent with immunofluorescent studies indicating increased GluR1, but not GluR2, subunit protein levels in cytosolic, crude membrane and PSD-enriched fractions from CA1 minislices. As with LTP, the FZP-withdrawal-induced GluR1 incorporation into CA1 neuron membranes may require the GluR1-trafficking protein, SAP97, which was also elevated in membrane-associated fractions. Together, our findings provide evidence that during FZP withdrawal, increased membrane incorporation of GluR1-containing AMPARs and associated upregulation of AMPAR functions in hippocampal CA1 pyramidal neurons share fundamental

similarities with the mechanisms underlying LTP. This implies that glutamatergic neuronal remodeling observed in LTP also subserves physiological adaptations to drug withdrawal.

Introduction

Remodeling of glutamatergic neurotransmission has recently been associated with dependence on and addiction to various drugs of abuse (Nestler, 2005), including the benzodiazepines (Izzo et al., 2001; Van Sickle et al., 2004; Xiang and Tietz, 2007). Benzodiazepines are widely prescribed anxiolytics and hypnotics, but have more limited clinical use as anticonvulsants due to the development of tolerance, largely mediated by dysfunction of gamma-amino butyric acid type A ($GABA_A$) receptors, the site of benzodiazepine allosteric actions (Zeng and Tietz, 1999; Bateson, 2002). Abrupt benzodiazepine withdrawal causes anxiety and insomnia, which can lead to drug self-administration and contribute to benzodiazepine misuse and abuse (Griffiths and Johnson, 2005). Recent evidence suggests that the benzodiazepine withdrawal syndrome is related to the regulation of the glutamatergic system (Izzo et al., 2001; Bateson, 2002; Van Sickle and Tietz, 2002; Van Sickle et al., 2004; Xiang and Tietz, 2007). The amplitudes of alpha-amino-3-hydroxy-5-methyl-4-isoxazole propionate receptor (AMPAR)-mediated miniature excitatory postsynaptic currents (mEPSCs) and AMPAR specific binding were increased in hippocampal CA1 pyramidal neurons after FZP withdrawal (Van Sickle and Tietz, 2002), associated with anxiety-like behavior in the elevated plus maze (Van Sickle et al., 2004; Xiang and Tietz, 2007). The strengthening of CA1 neuron excitatory synaptic function and the expression of anxiety were mitigated by prior pharmacological antagonism of AMPAR upregulation, underscoring the association of these neurophysiological and behavioral changes (Van Sickle et al., 2004; Xiang and Tietz, 2007). However, the exact mechanisms by which glutamatergic neurotransmission is enhanced during benzodiazepine withdrawal are not well understood.

Enhanced glutamatergic neurotransmission in CA1 neurons also occurs during long-term potentiation (LTP). The molecular mechanisms underlying LTP have been thoroughly studied and similar mechanisms may play a role in long-term drug effects, including dependence and addiction (Nestler, 2005). Increased glutamatergic strength during LTP primarily results from enhanced function of ionotropic AMPARs (Liu and Cull-Candy, 2000; Soderling and Derkach, 2000). Activity-dependent AMPAR trafficking between the plasma membrane and intracellular compartment (Malinow and Malenka, 2002) and rapid translocation between synaptic and extra-synaptic regions (Borgdorff and Choquet, 2002) are two mechanisms crucial to this form of plasticity. In addition, increased AMPAR expression, phosphorylation status and switches in AMPAR subunit composition can also contribute (Liu and Cull-Candy, 2000; Soderling and Derkach, 2000).

In rat hippocampus, three AMPAR subpopulations are expressed: GluR1 homomers, GluR1/2 and GluR2/3 heteromers (Wenthold et al., 1996). The AMPAR GluR1 subunit is essential for neuronal plasticity, since the presence of a GluR1 subunit alone was sufficient to sustain plasticity in GluR2/3 double knockout mice (Meng et al., 2003). GluR1 homomers that lack GluR2 subunits are permeable to calcium and susceptible to spermine blockade, thus show inward rectification at positive holding potentials (Lerma et al., 1994). Recombinant AMPARs show a graded inward rectification proportional to the number of functionally expressed non-GluR2 to GluR2 subunits (Washburn et al., 1997). Glutamate-activated AMPAR currents in hippocampal CA1 pyramidal neurons with a heterogeneous complement of primarily GluR2-containing AMPARs (Wenthold et al., 1996) show predominantly outward rectification (Lerma et al., 1994).

To further explore the molecular mechanisms underlying enhanced glutamatergic strength in CA1 neurons during benzodiazepine withdrawal, we used whole-cell electrophysiological recordings, confocal immunofluorescent imaging and immunoblot approaches to examine synaptic and extrasynaptic AMPAR channel properties and AMPAR subunit composition and distribution, using our well-established FZP withdrawal model (Van Sickle et al., 2004; Xiang and Tietz, 2007). We show that FZP withdrawal enhances GluR1 subunit expression, directs GluR1-containing AMPARs, including both GluR1 homomers and GluR1/2 heteromers, to extrasynaptic and synaptic sites on hippocampal CA1 pyramidal neurons. Moreover, this delivery may be promoted by synapse-associated protein 97 (SAP97), directing GluR1 subunit redistribution (Leonard et al., 1998; Sans et al., 2001).

The findings implicate enhanced AMPAR function and associated CA1 neuron hyperexcitability during FZP withdrawal (Van Sickle et al., 2004; Xiang and Tietz, 2007), as a potential substrate of physical dependence, a mechanism that shares fundamental characteristics with other forms of neuronal plasticity.

Materials and Methods

Chronic FZP treatment. All methods were approved by the University of Toledo College of Medicine (formerly the Medical University of Ohio), Institutional Animal Care and Use Committee (IACUC) and conformed to National Institutes of Health guidelines. A standard 1-week FZP treatment was carried out as previously established which reliably enhances AMPAR function (Van Sickle and Tietz, 2002; Van Sickle et al., 2004; Xiang and Tietz, 2007). Male Sprague–Dawley rats (Harlan, Indianapolis, IN), P36-42 at the time of study, were first adapted 2-4 days to 0.02% saccharin vehicle to disguise the bitter taste of FZP. Rats were then offered FZP (provided by the National Institute on Drug Abuse Drug Supply Program) in the vehicle for 1 week (100 mg/kg for 3 days, 150 mg/kg for 4 days) as their sole source of drinking water, followed by 2 days of drug withdrawal. The drug concentration offered is incremented from 100 to 150 mg/kg to avoid further aversion to the drug. Daily water consumption was monitored to adjust drug concentration based on the volume consumed. The actual dose achieved was calculated and rats that did not achieve a criterion dose of a weekly average of 120 mg/kg/day were excluded. During drug withdrawal, rats received saccharin water. Control rats received saccharin vehicle in parallel. All electrophysiological and immunochemical studies were conducted with the observer blind to the experimental treatment. This dosing regimen reliably induces manifestations of both benzodiazepine tolerance and dependence (Tietz et al., 1999a; Zeng and Tietz, 1999; Van Sickle et al., 2004; Xiang and Tietz, 2007). Rats treated in this way show a progressive increase in AMPA mEPSC amplitude from day 1 (~15%) to day 2 (~30%) after benzodiazepine withdrawal. Both the increase in AMPAR function and the associated anxiety-like behavior are transient and return to

control levels within 4 days after treatment cessation (Van Sickle et al., 2004).

FZP is prescribed as a hypnotic at doses 6 times lower than diazepam, reflecting differences in its clinical potency and bioavailability (Chouinard, 2004) and is a full agonist at recombinant $GABA_A$ receptors with a relative potency ~10 times lower than diazepam (Downing et al., 2005). Thus, the concentration of FZP (100-150 mg/kg) offered to rats is appropriate to its relative potency. When expressed in diazepam equivalents, 1-week FZP treatment results in brain levels of FZP and its active metabolites equivalent to 0.6 μM diazepam, as determined by radioreceptor assay (Xie and Tietz, 1992), comparable to that reported for other typical chronic diazepam treatments (Izzo et al., 2001). Due to the short half-life of FZP in rat brain (<12 hr), the FZP level is negligible in the hippocampus 2 days after FZP withdrawal (Xie and Tietz, 1992; Van Sickle et al., 2004).

Hippocampal tissue preparation for electrophysiology. For acutely isolated neurons, coronal half-brain sections (400 μm) were prepared on a vibraslicer (Campden Instrument, Ltd. Lafayette, IN) in ice-cold, pre-gassed (95% O_2/5% CO_2) Ca^{2+}-free PIPES solution containing (mM): NaCl 120; KCl 2.5; $MgCl_2$ 1; glucose 25; PIPES 20 (pH 7.4, 305 mOsm). For *in vitro* recordings, transverse hippocampal slices (400 μm) were prepared on a vibratome (Ted Pella, Inc., Redding, CA) as previously described (Van Sickle et al., 2004) in low Ca^{2+}-high Mg^{2+} dissection buffer then maintained ≥ 1 hr in artificial cerebral spinal fluid (ACSF, in mM: NaCl, 119; KCl, 2.5; $CaCl_2$, 1.8; $MgSO_4$, 1.0; NaH_2PO_4, 1.25; $NaHCO_3$, 26; D-glucose, 10; pH 7.4) prior to whole-cell recording at room temperature.

Acute neuron isolation for electrophysiology. Coronal slices were maintained at room

temperature for >1 hr in gassed PIPES then digested in 1.4 units/ml protease XIV (Sigma-Aldrich Corp., St Louis, MO) in PIPES buffer at 32 °C for 40 min. After a wash in 0.1 % BSA and then in PIPES, the hippocampus was dissected on ice. CA1 minislices were notched on the dorsal and ventral edges, and followed by triturating in 100 µl PIPES using a 22, then 30 gauge pipette. The supernatant was removed and plated onto acid-washed coverslips. Cells were allowed to attach 15 min before use.

Whole-cell recording in isolated neurons. AMPAR currents were recorded in dissociated neurons in external solution, including (mM) NaCl 154; $CaCl_2$ 2; KCl 2.5; $MgCl_2$ 2; glucose 10; HEPES 10 (pH 7.35, 315 mOsm) with 200 µM $CdCl_2$ and 0.5 µM tetrodotoxin (TTX, Sigma) to block voltage-gated Ca^{2+} and Na^{+} channels. Neurons were selected by their relative size and pyramidal morphology as previously described (Tietz et al., 1999b). Elliptical shaped, very large or bipolar neurons were excluded. The borosilicate micropipette (4-6 MOhm, Sutter Instruments, Novato, CA) internal solution contained (mM): $CsCH_3SO_3$ 115; CsCl 20; HEPES 10; $MgCl_2$ 2.5; EGTA 0.6; Na_2ATP 4; NaGTP 0.4; Na_2phosphocreatine 10; as well as 50 units/ml creatine phosphokinase (pH 7.25, 295 mOsm). Bath application of 100 µM DL-2-amino-5-phosphopentanoic acid (APV, Sigma) was used to block N-methyl-D-aspartate receptor (NMDAR) currents activated by glutamate. Whole-cell recordings with ultra-fast drug application were performed at 22 °C on lifted, isolated CA1 pyramidal cells, similar to Mayer *et* al. (Partin et al., 1996). Drugs were applied to lifted cells positioned near the adjacent opening of a three-barrel square-tip pipette, coupled to a fast-stepper device (Warner Instruments, Hamden, CT). Each barrel is ~7 times larger (~160 µm) than the dissociated CA1 neuron allowing for sufficient drug

exposure. Transition time (20-80%, 0.09-0.47 ms) was estimated with the open-tip patch electrode response to a rapid solution change from normal (2.5 mM) to 100 mM external KCl at the end of the experiment. These application rates were previously shown to be sufficient for detection of whole-cell AMPAR currents and evaluation of AMPAR current kinetics (Partin et al., 1996).

The degree of inward rectification of currents elicited by glutamate or kainate application to acutely isolated neurons or by endogenous glutamate release onto CA1 neurons in hippocampal slices, was used to evaluate the effect of benzodiazepine withdrawal on the proportion of GluR2-lacking to GluR2-containing AMPARs at extrasynaptic and synaptic sites (Washburn et al., 1997). In hippocampal neurons as in heterologous expression systems, GluR2-containing AMPARs, due to the Q residue at the Q/R RNA editing site in the intra-membrane domain, are resistant to spermine blockade and show linear I-V relationships or outward rectification in a voltage- and activity-dependent manner. Conversely, AMPARs lacking the GluR2 subunit are susceptible to spermine blockade and show inward rectification at positive holding potentials (Lerma et al., 1994). All of the widely used AMPAR agonists, including glutamate and AMPA, evoke strong desensitization of the receptor, with the exception of kainate (Patneau and Mayer, 1991). Importantly, kainate responses in CA1 neurons can also be completely blocked by the AMPA antagonist, GYKI 53655 [7H-1,3-Dioxolo(4,5-H) (2,3) Benzodiazepine-7-Carboxamide,8,9-Dihydro-5-(4-Aminophenyl),8-Dimethyl-Monohydrochloride] (Seifert et al., 2000). Therefore, rectification studies were carried out during both ultra-rapid application of glutamate and prolonged exposure to kainate with spermine in the micropipette. To facilitate rapid cell dialysis, spermine (100 μM, Sigma) was contained in the tip solution and the micropipette was

then backfilled with the spermine-containing internal solution. Currents were elicited by 1 ms application of 2 mM glutamate (V_H = -60 and +40 mV) onto lifted cells or during 6 s exposure to 300 μM kainate during a voltage ramp (V_H = -100 through +80 mV, 1 mV/ms ramp) to avoid AMPAR desensitization. Voltage-ramp currents were recorded on the same cell before and during kainate application. The kainate-induced I-V curve was obtained by subtracting the former from the latter currents.

Polyamines, like 1-naphthylacetyl spermine (NAS), which carry a bulky hydrophobic head group, either too large to permeate the narrow part of the pore and/or bind to a hydrophobic region in the channel, are much more potent AMPAR inhibitors than spermine itself (Stromgaard and Mellor, 2004). Therefore, NAS (100 μM, Sigma) was co-applied (2 s) extracellularly to inhibit currents elicited by sustained (6 s) application of kainate (300 μM, Ocean Produce International, Canada).

Currents were low-pass filtered at 5 kHz (Axoclamp 200A, Axon Instruments) and digitized at 10-20 kHz (Digidata 1322, Axon Instruments, Foster City, CA). The series resistance was compensated at least >85%. Whole-cell responses from isolated neurons (Table 1) were analyzed off-line from digitized current traces using Clampfit (Axon Instruments Inc., Foster City, CA) and GraphPad Prism (GraphPad Software Inc., San Diego, CA). Peak current (pA) was defined as the initial maximal negative deflection from the baseline value determined immediately before the onset of the drug response. To avoid current variances due to differences in cell size, current density (pA/pF) was set as peak current amplitude (pA) divided by membrane capacitance (pF) from the same cell. The rise and decay kinetics of the AMPA currents were measured following

application of a 1 ms pulse of 2 mM glutamate, while a 180 ms application was delivered for the measurement of desensitization kinetics. The rise and decay times were determined from 10% to 90% of the AMPA current rising phase or decay phase, respectively. The time constant (τ) of desensitization was fit by a one component exponential equation:

$$[\ f(t) = \sum_{i=1}^{n} A_i \exp(e \exp(-t/\tau_i)) + C\ ] \text{ (equation I).}$$

Concentration-response curves were fit by non-linear regression [sigmoidal dose-response (variable slope):

$$I = I_{min} + (I_{max} - I_{min})/(1 + 10\text{^}((\text{LogEC}_{50} - \text{Log[glutamate]}) \times \text{HillSlope}))] \text{ (equation II).}$$

The rectification index was defined as peak current amplitude at a holding potential of +40 mV divided by that at -60 mV. For analysis of voltage ramps during kainate application, the ratio of the ramp slope measured around +40 (+35 to + 45) and -60 (-65 to -55) mV was calculated. A linear I-V relationship yielded a ratio = 1; while ratios > 1 or < 1 were indicative of outward or inward rectification, respectively. Kainate-induced current density was also measured at V_H = -60 mV.

Whole-cell recording in hippocampal slices. For recording of action potential-independent, AMPAR-mediated miniature EPSCs, hippocampal slices were perfused (2.5 ml/min) at room temperature with gassed ACSF. Patch pipettes (5–9 MOhm) were filled with internal solution containing (in mM): $CsCH_3SO_3$, 132.5; CsCl, 17.5; HEPES, 10; Ethylene glycol-bis(2-aminoethylether)-N,N,N′,N′-tetraacetic acid (EGTA), 0.2; NaCl, 8; Mg-ATP, 2; Na_3-GTP, 0.3; N-(2,6-Dimethylphenylcarbamoylmethyl)triethylammonium bromide (QX-314), 2; spermine, 0.1, pH 7.2 adjusted with CsOH. Resting membrane potential (RMP) was measured

immediately upon cell break-in and was invariant between groups (Table 2). Cells in which the holding current changed by more than 20% or the seal degraded were abandoned. Neurons were voltage-clamped (V_H -60 to +40 mV) in continuous mode (cSEVC) using an Axoclamp 2A amplifier (Axon Instruments Inc.). Baseline mEPSC activity was recorded for at least 8 min with 1 μM TTX, 25 μM (3-aminopropyl)(diethoxymethyl) phosphinic acid (CGP-35348), 50 μM picrotoxin and 50 μM APV. Current output, monitored online (PClamp 9.0 Software, Axon Instruments Inc.), was low-pass filtered (10 kHz), amplified 100×, DC offset and then digitized at 20 kHz (Digidata 1320A, Axon) for later analysis.

Miniature EPSC events were detected and averaged using MiniAnalysis software (Synaptosoft Inc., Leonia, NJ). Peak current amplitude was derived from averaged events aligned by rise time (< 5 mS). Peak mEPSC amplitude and current kinetics were estimated using a single exponential function:

$$y(t) = a\exp(-t/t) \text{ (equation III).}$$

The rectification index in CA1 neurons from hippocampal slices was defined as in isolated neurons.

Immunofluorescence studies. For confocal imaging of surface GluR1 and GluR2 subunits, and SAP97 antibody immunofluorescence, 5 mm hippocampal blocks were post-fixed in 4% paraformaldehyde in 0.1 M PB at 4°C overnight after decapitation. For dual labeling of surface N-GluR1/N-GluR2, non-permeablizing conditions were used on free-floating coronal slices (40 μm). After blocking with 10% donkey serum, signals were detected with a rabbit antibody against the amino terminal of the GluR1 subunit (N-GluR1 antibody, 1:5, Calbiochem, Germany) and a

mouse antibody directed against the amino terminal of the GluR2 subunit (N-GluR2 antibody, 1:250, Chemicon), and then visualized with an Alexa 488-conjugated donkey anti-rabbit antibody for N-GluR1 (1:500, Molecular Probes, Eugene, OR) and an Alexa 594-conjugated donkey anti-mouse secondary antibody for N-GluR2 (1:500, Molecular Probes). For SAP97 analysis, tissue was permeabilized with 0.1% Tween20. After blocking with 10% donkey serum, slices were incubated at first with a rabbit anti-SAP97 antibody (1:250, Affinity BioReagents, Golden, CO), and followed by incubation with an Alexa 488-conjugated donkey anti-rabbit antibody (1:500). Experimental controls to verify antibody specificity included antigen pre-absorption, omission of primary antibodies, host-matched γ-globulin or incubation with detergent. This penetration with detergent has been reliably applied for detecting total antibody signal, including that associated with cytoplasmic and membrane compartments. Omission of detergent was designed to assess surface signal. Sections were visualized and quantified using an Olympus BX51WI microscope (Olympus America Inc., Melville, NY), coupled to a Radiance 2000 laser scanning confocal system (Bio-Rad, Hercules, CA) with constant laser power, gain, iris and offset settings between samples. All data collection and analysis were conducted with the observer unaware of experimental group.

Immunofluorescence labeling on confocal images was assessed using ImageJ software (National Institutes of Health, Bethesda, MD). To avoid cross-talk between channels, we acquired green and red signals separately within a given area of the same sections using different filters. The intensity of immunofluorescence was determined from the average grey scale value. Appropriate areas of interest were used to analyze the immunofluorescence signals: stratum pyramidale (*sp*)

GluR1 and GluR2, somatic membrane area; stratum radiatum (*sr*) GluR1 and GluR2, dendrite area; *sp* SAP97, entire cell body. Mean density (integrated density/μm^2) measurements were obtained using ImageJ Software. N-GluR1/2 colocalization signals were highlighted with the colocalization tool. The threshold was optimized to highlight only the area of colocalization and was held constant among samples and experimental groups. Particle mean density and particle number were standardized to cell circumference (*sp*) or dendrite length (*sr*) (μm).

Subcellular fractionation and immunoblotting. Fractionation methods were modified from those of (Smith et al., 2006), to yield P2 and P3 fraction relatively enriched in PSDs, as confirmed by PSD-95 (Chemicon, Temecula, CA) immunoblotting. All procedures were conducted at 0-4°C. Hippocampi were rapidly dissected from matched pairs of control and FZP-withdrawn rats and the CA1 region microdissected from 2-3 mm hippocampal slices, was immediately submerged in ice-cold homogenization buffer [10 mM Tris, pH 7.4, 320 mM sucrose, 1 mM ethylenedinitrilotetraacetic acid (EDTA), 1 mM EGTA, 5 mM NaF, 1 mM sodium orthovanadate, 1 μM cyclosporine A, 0.5 μM okadaic acid, 1% protease inhibitor (Sigma)]. Homogenates were centrifuged at 960 X g for 10 min to remove large debris. The supernatant (S1) was then centrifuged at 10,000 X g for 30 min to obtain the crude membrane pellet (P2) and cytosol (S2). The PSD-enriched fraction (P3) was obtained by incubating P2 pellets in Triton-homogenate buffer on ice for 20 min and then centrifuging at 32,000 X g for 1 hr. Proteins in S2 were precipitated with acetone at - 20 °C for more than 2 hr, centrifuged at 3,000 X g for 30 min and air dried. Final pellets were sonicated in resuspension buffer (10 mM Tris, pH 8, 1 mM EDTA, and 1% SDS). Protein concentrations were determined with a BCA protein assay kit (Pierce, Rockford,

IL).

Ten or fifteen micrograms of protein per well was mixed with sample buffer [Laemmli sample buffer (Bio-RAD, Hercules, CA) plus 5% β-mercaptoethanol] and running buffer (25 mM Tris base, 200 mM glycine, 0.1% SDS) then loaded on a 10% polyacrylamide gel. Protein was wet-transferred to a nitracellulose membrane. Primary antibodies were incubated with membranes overnight at 4°C. The antibody signal was detected with horseradish peroxidase (HRP)-coupled secondary antibodies (1:10,000/20,000, Jackson ImmunoResearch Inc, West Grove, PA), followed by enhanced chemiluminescence (ECL) (Denville Scientific Inc., Metuchen, NJ). All P2 and S2 fractions were conducted under the same conditions simultaneously to obtain P2/S2 density ratios. P3 fractions were run separately. Primary antibodies used included: anti-GluR1 (1:400, Santa Cruz biotechnology, CA), anti-GluR2 (1:500 or 1:1000, Molecular Probes) and anti-SAP97 (1:4000, Stressgen Biotechnologies, Canada) anti-actin (1:20,000, Chemicon). Images of immunoblots were scanned and immunoreactivity quantified with UN-SCAN-IT (ver 6.1, Silk Scientific, Orem, UT). Each antibody signals were normalized to the corresponding actin signal.

Statistical analyses. Data are reported as mean ± SEM and the significance level was set at $p < 0.05$. Error bars represent the standard error of the mean (SEM). Deviations from normality and homogeneity of variance were determined by Shapiro-Wilk test and F test, respectively. Statistical differences were determined by unpaired two-tailed Student's *t*-test, or alternately Mann-Whitney U test when samples were not normally distributed.

Results

Synaptic and extrasynaptic AMPAR function is increased in response to FZP withdrawal. To investigate AMPAR channel properties, acutely isolated CA1 pyramidal neurons and hippocampal slices were prepared from control and 2-day FZP-withdrawn rats. AMPARs desensitize rapidly in the continued presence of agonist (Patneau and Mayer, 1991), limiting kinetic analysis. To avoid this problem, whole-cell recordings were first performed on lifted, isolated CA1 neurons (Fig. 1*A*), using ultra-rapid application of a saturating concentration (2 mM) of glutamate for 1 ms. Neurons from FZP-withdrawn rats showed enhanced AMPAR function, an increase in current density (pA/pF), i.e. current amplitude normalized by cell size, compared to controls. In some studies, excised patches have been used to investigate AMPAR kinetics. However, outside-out patch recordings may be misleading due to sampling errors, since individual patches will contain only a small sample of membrane from the soma or primary dendrites, and may contain either synaptic or extrasynaptic receptors. Therefore, whole-cell recordings rather than outside-out patch recordings were preferable to assess the physiological changes in both synaptic and extrasynaptic cell surface AMPAR populations on both soma and proximal dendrites. There were no significant alterations in membrane capacitance, access resistance, rise time or decay time between CON and FZP groups (Fig. 1*B* and *C*; Table 1). These results suggest that the function of both extrasynaptic and synaptic AMPARs may be upregulated in response to FZP withdrawal, though the contribution of synaptic AMPARs is uncertain.

To better address whether synaptic AMPAR function is augmented, whole-cell recordings were also performed in intact pyramidal neurons in hippocampal slices. Consistent with the former

findings in isolated neurons, we also observed a significant increase in AMPAR mEPSC amplitude at V_H = -60 mV, without a change in current kinetics (Table 2). These results are also compatible with previous mEPSCs recordings in CA1 neurons in hippocampal slices from FZP-withdrawn rats (Van Sickle and Tietz, 2002; Van Sickle et al., 2004; Xiang and Tietz, 2007). Collectively, these findings suggest that FZP withdrawal facilitates both extrasynaptic and synaptic AMPAR function.

Molecular mechanisms underlying the progressive increase in AMPAR function observed during FZP withdrawal could include one or several of the following AMPAR modifications: 1) altered channel kinetic properties, 2) increased glutamate affinity or efficacy, 3) increased membrane insertion of receptors, or 4) changes in AMPAR subunit composition or phosphorylation status. To further investigate channel kinetic properties, AMPAR desensitization was measured using prolonged glutamate application (180 ms) on lifted isolated neurons. There was no significant difference in tau of desensitization (τ_{des}: CON 41.4 ± 4.0 *vs*. FZP 40.8 ± 4.4) (Fig. 1 *E* and *F*), suggesting that altered whole-cell channel kinetics may not account for potentiation of AMPA currents during FZP withdrawal.

To address changes in glutamate affinity and efficacy at AMPARs during FZP withdrawal, glutamate concentration-response studies were conducted on lifted, isolated CA1 neurons. At saturating concentrations, from 500 μM to 3000 μM, neurons from the FZP-withdrawn group exhibited significantly increased AMPAR current density (Fig. 1*G* and *H*). Analysis of individual fits of concentration-response data revealed that average maximal current density (I_{max}) was significantly augmented during FZP withdrawal (CON: 161.7 ± 24.2 pA/pF; FZP 233.4 ± 19.3

pA/pF, $p < 0.05$). A statistical comparison of log EC_{50} values (CON: -3.74 ± 0.08 M; FZP -3.58 ± 0.07 M, $p > 0.05$) indicated no change in glutamate EC_{50} (CON: 210 ± 36 μM; FZP 282 ± 36 μM, $p > 0.05$), suggesting there was no change in glutamate affinity. Since the increased AMPAR current density was observed at saturating glutamate concentrations, an increase in the number of functional AMPARs at the cell surface rather than altered glutamate affinity or efficacy, is chiefly responsible for the enhanced AMPAR function.

Functional incorporation of GluR2-lacking AMPARs in response to FZP withdrawal. A switch in AMPAR subunit composition has been observed after many forms of neuronal activation (Liu and Cull-Candy, 2000). To determine whether such changes occur during FZP withdrawal, the current-voltage relationship (*I-V*) of CA1 neuron AMPA currents was evaluated in both isolated CA1 neurons and neurons in hippocampal slices. Inward rectification in the presence of intracellular spermine has been used as a measure of the proportion of GluR2-lacking AMPARs on CA1 neurons, both in culture and in organotypic hippocampal slices following tetanic stimulation of Schaffer collaterals (Shi et al., 1999; Esteban et al., 2003). Isolated neurons from the FZP-withdrawn group showed a moderate decrease in the rectification index (peak amplitude at +40 mV/ peak amplitude at -60 mV) following rapid (1 ms, 2 mM) glutamate application (CON: 0.56 ± 0.04 *vs.* FZP: 0.46 ± 0.03, $p < 0.05$) (Fig. 2*A* and *B*), consistent with the degree of change in other pathological conditions (Washburn et al., 1997), though smaller than that reported in CA1 neurons following transient overexpression of GluR1 (or GluR4) subunits (Shi et al., 1999; Esteban et al., 2003). Miniature synaptic currents recorded from CA1 neurons in hippocampal slices from FZP-withdrawn rats also showed a decreased +40/-60 rectification index (CON: 0.76 ±

0.03 *vs.* FZP: 0.60 ± 0.04) (Fig. 2*C* and *D*). Together, the findings suggest a relative increase in both extrasynaptic and synaptic GluR2-lacking AMPARs during FZP withdrawal, which likely represent GluR1 homomers.

Since kainate is the only AMPAR agonist with a minimal capacity to induce desensitization and since at this age (P36-42) more than 95% of kainate-induced currents in CA1 neurons are due to AMPAR activation (Seifert et al., 2000), we applied kainate on CA1 neurons to further characterize the *I-V* properties of altered AMPA currents. There was a clearly observable (Fig. 2*E* and *F*) negative shift in the slope ratios derived from individual pyramidal neurons responses to a voltage ramp (-100 to + 80 mV) during kainate application (CON slope ratio: 1.44 ± 0.08, n = 14; FZP slope ratio: 1.15 ± 0.03, n = 21, $p < 0.001$). Eleven of fourteen (71%) control neurons were outwardly rectifying (1.2-2.1) while the remainder (4/14) had rectification indices between 1.1 and 1.2. In contrast, 4 of 21 FZP-withdrawn neuron responses were inwardly rectifying with slope ratios <1.0 (0.83-0.95), while 16 had rectification indices between 1.0 and 1.2. One FZP-withdrawn cell exhibited outward rectification with a slope ratio of 1.39.

GluR1-containing AMPARs are specifically blocked by polyamines and several toxins. Due to the absence of a bulky hydrophobic head group, spermine is much less potent than the joro-spider toxin analogue, NAS and the digger wasp venom derivative, philanthotoxin 343 (Stromgaard and Mellor, 2004). Thus in the current study, the presence of GluR1-containing AMPARs was further assessed pharmacologically with NAS. NAS was applied extracellularly during prolonged kainate exposure on acutely isolated neurons. Consistent with its relatively greater potency to block GluR2-lacking AMPARs (Stromgaard and Mellor, 2004), neurons from the FZP-withdrawn group

JPET Fast Forward. Published on May 17, 2007 as DOI: 10.1124/jpet.107.121798
This article has not been copyedited and formatted. The final version may differ from this version.

showed a sizeable (71%) NAS blockade of kainate-induced AMPA currents compared with a small, though detectable (16%) blockade in neurons from the control group (Fig. 2*G* and *H*). Though the relative potency of spermine to block applied and exogenous glutamate can not be directly compared to NAS blockade of 300 μM kainate currents, this observation is also consistent with the findings of rectification studies employing spermine in the micropipette. Together, these findings are all in agreement with a major contribution of GluR2-lacking AMPARs, possibly GluR1 homomers to the augmented AMPAR response during benzodiazepine withdrawal.

Delivery of synaptic and extrasynaptic CA1 neuron GluR1 subunits in response to FZP withdrawal. Rectification studies suggested an increase in membrane incorporation of GluR1 homomers during FZP withdrawal. However, the relative contribution of an increase in surface GluR1 homomers or GluR1/2 heteromers to AMPAR potentiation is unclear. Moreover, GluR1 subunit membrane incorporation may result from the regulation of receptor expression or redistribution of existing receptors. To address these questions, confocal immunofluorescence analysis was performed in hippocampal slices.

To detect whether GluR1 and/or GluR2 subunit surface incorporation was altered in response to FZP withdrawal, dual-immunofluorescence confocal imaging studies of anti-amino terminal (N-terminal) GluR1 and GluR2 antibodies were carried in somatic and dendritic region of the CA1 area (Fig. 3*A*) under non-permeablizing conditions, the most practical available approach to label surface AMPAR subunits. Experimental conditions were validated by gamma globulin (Fig. 3*B*) and permeablization controls (see Supplemental Data). A marked increase in GluR1 signal as well as GluR1/2 colocalization was observed in CA1 neuron somata (*sp*, Fig. 3*C*) and apical dendrites

(stratum radiatum, *sr*, Fig. 3*D*), but not basal dendritic regions (stratum oriens, *so*, data not shown). The increased GluR1 signal in *sr*, but not in *so* agrees with recent preliminary studies that showed a differential distribution of GluR1 homomers in apical *vs*. basal dendrites (Bagal et al., 2005, Soc. Neurosci. Abstr.). No differences were detected in surface GluR2 signal in somatic or dendritic areas (Fig. 3*C* and *D*, middle panels), suggesting that a change in GluR2 subunit surface expression is not involved in AMPAR potentiation during FZP withdrawal. Quantification of signal intensity (Fig. 3*E* and *F*) revealed that surface GluR1 signal was augmented more than GluR1/2 colocalization in *sp* (mean density increase: 64% *vs*. 26%) and *sr* (mean density increase: 71% *vs*. 45%), indicating that GluR1 subunits were inserted in somatic or apical dendritic membranes during FZP withdrawal as GluR1 homomers and GluR1/2 heteromers. Given the absence of alterations in surface GluR2 labeling, the observation that GluR1/2 colocalization was also enhanced suggests that membrane-inserted AMPARs might be reassembled from the GluR2/3 AMPAR subpopulation into GluR1/2 heteromers. Nevertheless, other possibilities such as synaptic delivery of homomeric GluR1 AMPARs adjacent to existing GluR2-containing receptors cannot be excluded.

To corroborate immunofluorescence studies, immunoblot analyses of subcellular CA1 neuron fractions were undertaken. Three subcellular fractions were collected from hippocampal CA1 minislices and used in this study, including S2 (cytosol), P2 (crude membrane) and P3 (PSD-enriched) fractions. An enrichment of PSD-95 signal was demonstrated in the P3 vs. the P2 fraction (Fig. 4). There were significant increases in GluR1 immunoreactivity in cytosolic and crude membrane fractions in response to FZP withdrawal (Fig. 5*A*), suggesting that total GluR1

protein expression was augmented and may contribute to the elevated surface GluR1 incorporation. Moreover, a 57% increase in the amount of GluR1 in the PSD-enriched, P3 fraction was found in membranes from FZP-withdrawn as compared to control rats (Fig. 5*A*), which support the electrophysiological findings and suggest that more GluR1 homomers may be inserted in synaptic membrane. In contrast to the increased GluR1 signal density, no alterations in the amount of GluR2 protein were found in any fraction after FZP withdrawal (Fig. 5*B*), in agreement with the lack of change in GluR2 immunofluorescence labeling. Meanwhile, the P2/S2 ratio of both GluR1 and GluR2 subunits was unaltered in CA1 minislices from the FZP vs. the control group (GluR1 P2/S2: CON 1.09 ± 0.11, FZP 1.14 ± 0.18; GluR2 P2/S2: CON 1.58 ± 0.30, FZP 2.23 ± 0.58, $p > 0.05$). Collectively, our immunochemical data suggest that enhanced AMPAR GluR1 subunit expression but not redistribution contributes to AMPAR membrane incorporation and subsequent receptor potentiation during FZP withdrawal. Taken together, the findings suggest that enhanced GluR1 subunit expression and subsequent membrane delivery, rather than elevated GluR2 degradation, may result in increased GluR1 homomer incorporation into extrasynaptic and synaptic membranes, since neither total GluR2 protein level nor its P2/S2 ratio were changed after FZP withdrawal.

SAP97 may promote GluR1 membrane delivery in response to FZP withdrawal. The increase in GluR1-containing cell surface AMPARs observed with FZP withdrawal is similar to that observed with LTP, and we thus sought to determine whether other similar mechanisms might be involved. In LTP, GluR1-containing AMPAR trafficking depends on interactions between the C-terminus of the GluR1 subunit and type I (PSD-95, Dlg and ZO-1) PDZ domain-containing

proteins, such as SAP97 (Leonard et al., 1998). SAP97, a 97 kDa postsynaptic PDZ protein, demonstrated to specifically associate with GluR1, but not other AMPAR subunits (Leonard et al., 1998). SAP97 was shown to act in the early secretory pathway of membrane-targeted GluR1-containing AMPARs (Sans et al., 2001). To investigate if SAP97 may be involved in the control of GluR1-containing AMPAR trafficking during FZP withdrawal, immunofluorescence studies with an anti-SAP97 antibody were performed following membrane permeablization. Cytoplasmic SAP97 clusters were more dense than observed in dendrites, and a significantly increased SAP97 signal (20%) was apparent in *sp*, but not *sr* of the FZP-withdrawn group (Fig. 6*A*). There was no change in SAP97 signal in basal dendrites (*so*) during FZP withdrawal (data not shown).

SAP97 protein level was further investigated by subcellular fractionation and immunoblotting. As seen in Fig. 6*B*, a significant upregulation of SAP97 expression was found in CA1 neuron P2 and P3 membrane components from FZP rats, with no apparent regulation in S2. Interestingly, the P2/S2 density ratio of anti-SAP97 labeled protein was significantly elevated (~45%) during FZP withdrawal. As S2 SAP97 was unaltered, the increased in SAP97 protein associated with crude membranes (P2) and those enriched in asymmetric synapses (P3), may indicate a possible role for SAP97 in facilitating GluR1-containing AMPAR trafficking to extrasynaptic and synaptic membranes during benzodiazepine withdrawal.

Discussion

AMPAR-mediated current potentiation and a switch in AMPAR subunit composition at the postsynaptic membrane are critical to activity-dependent changes in synaptic strength. The nature of regulated AMPAR trafficking in various forms of synaptic plasticity is well characterized (Shi et al., 1999), while its role in mediating long-term drug effects, in particular FZP withdrawal-induced glutamatergic remodeling, is unclear. In our previous studies, anxiety-like behavior was associated with increased CA1 neuron AMPAR function in FZP-withdrawn rats (Van Sickle et al., 2004, Xiang and Tietz, 2007). The current electrophysiological studies demonstrate that extrasynaptic and synaptic AMPAR currents were both significantly enhanced during benzodiazepine withdrawal with no change in AMPAR channel properties. The relative shift towards inward rectification of AMPAR-mediated currents in the presence of polyamines indicates a substantial contribution of GluR2-lacking AMPARs to the increased AMPAR potentiation during FZP-withdrawal. Immunofluorescence studies and immunoblot analysis revealed increases in extrasynaptic and synaptic GluR1 signals with an increase in the total amount GluR1 protein, collectively suggesting that FZP-withdrawal promotes the expression of GluR1 subunits, as well as the delivery of GluR1 homomers into somatic and apical dendritic membranes and synapses. Concomitant with the increased level of GluR1 in P2 and P3 fractions, FZP withdrawal also promotes SAP97 expression, which may favor GluR1 subunit release from the endoplasmic reticulum (ER) and drive GluR1 subunits into membranes/synapses. Moreover, the significant increases in membrane association of SAP97 and a shift of SAP97 from the S2 to the P2 fraction further supports the notion that SAP97 redistribution may be an important step for

GluR1 membrane/synapse delivery during FZP withdrawal, as with other forms of activity-dependent plasticity. This is the first demonstration that FZP withdrawal promotes AMPAR membrane/synapse trafficking and subunit remodeling, leading to potentiation of AMPAR function, a mechanisms that is also central to LTP (Zamanillo et al., 1999; Shi et al., 2001; Malinow and Malenka, 2002). Moreover, the findings suggest that the mechanisms underlying activity-dependent hippocampal glutamatergic plasticity may be highly conserved and subserve the physiological adaptations that occur during drug withdrawal as well as other adaptive behaviors.

AMPAR channel characteristics and increased glutamatergic strength in response to FZP withdrawal. Enhancement of AMPAR function is the main phenomenon defining activity-dependent plasticity. LTP studies indicate that augmented AMPAR function could be related to alterations in AMPAR trafficking, receptor number, subunit composition, phosphorylation status, channel conductance and kinetics (Soderling and Derkach, 2000), among other possibilities. Both extrasynaptic and synaptic AMPAR-mediated currents elicited by exogenous and endogenous glutamate were augmented during FZP withdrawal. To explore the underlying mechanisms and evaluate the complement of AMPARs on cell membranes, AMPAR channel properties were investigated at the whole-cell level. Given that AMPARs desensitize very rapidly (in milliseconds), an ultra-rapid stepper system, which allowed millisecond agonist application onto cells lifted, was used to ensure nearly simultaneous receptor activation without desensitization. No evidence of alterations in AMPAR channel kinetic properties (rise time, decay and desensitization rates) was found after FZP withdrawal, consistent with other LTP studies

(Rammes et al., 1999). Therefore, channel kinetic properties are not a likely basis for increased glutamatergic strength induced by FZP withdrawal. Further single channel studies of somatic and dendritic membranes could help to clarify whether fundamental changes in AMPAR channel conductance or gating underlies AMPA current potentiation.

AMPAR membrane delivery increases glutamatergic strength in response to FZP withdrawal. Considerable evidence indicates that native AMPAR subunits have different trafficking patterns; GluR1-containing AMPARs are inserted into membranes in an activity-dependent manner, determined by interactions between GluR1 and type I PDZ proteins (Leonard et al., 1998; Sans et al., 2001), while GluR2-containing AMPARs are continuously cycled in and out of membranes, replacing existing receptors (Shi et al., 2001; Malinow and Malenka, 2002). These subunit-specific properties govern membrane delivery of AMPARs in response to neuronal activity. As in LTP, GluR1 membrane delivery requires the interaction between the PDZ binding domain of GluR1 and SAP97, the only PDZ protein known to interact specifically with the GluR1, but not other AMPAR subunits (Leonard et al., 1998). Our immunofluorescence studies demonstrated that surface GluR1 signal was augmented in *sp*, associated with increased SAP97 expression in the cell body, suggesting that SAP97 may be involved in facilitating release of GluR1 subunits from the ER and their further delivery to membranes/synapses. Nevertheless, immunofluorescence studies lack the sensitivity required to detect synaptic SAP97 incorporation and an increase in dendritic SAP97 signal was not detected in confocal imaging studies. In subfractionation studies, enhanced GluR1 levels were accompanied by upregulation of SAP97 in P2 and P3 fractions. An increase in the SAP97 P2/S2 ratio raises the

possibility that SAP97 may redistribute from the cytosol to the membrane or that locally synthesized SAP97 near the membrane might be enhanced. The membrane/synaptic relocalization of SAP97 was suggested to enable its participation in the regulation of AMPAR trafficking (Wu et al., 2002) and GluR-Ser^{845} phosphorylation (Colledge et al., 2000). Thus coupled with immunofluorescence studies, subfractionation studies suggest that similar mechanisms may be operative during FZP withdrawal resulting in potentiation of AMPAR function and the associated anxiety-like behavior (Van Sickle et al., 2004; Xiang and Tietz, 2007).

The relative contribution of extrasynaptic GluR1-containing AMPARs to glutamatergic strength is uncertain and may have contributed to the difference in the rectification indices calculated after glutamate application to dissociated neurons or endogenous glutamate release onto CA1 neuron synapses in slices. Several studies have suggested that GluR1-containing AMPARs at non-synaptic sites may also be important for plasticity, because functional AMPARs are expressed on CA1 somata and dendrites consistent with immunolabeling studies (Wenthold et al., 1996). Accordingly, large glutamate-evoked currents from nucleated CA1 somatic patches were nearly abolished in GluR1-deficient mice, reflecting a significant functional role for GluR1-containing AMPARs on CA1 cell bodies (Zamanillo et al., 1999). Despite the marked reduction in somatic AMPAR currents, these GluR1-deficient mice had normal AMPAR-mediated synaptic transmission; however, they could not sustain LTP (Zamanillo et al., 1999), confirming the importance of this subunit for activity-dependent plasticity and suggesting an important role for somatic GluR1-containing AMPARs in mediating increases in glutamatergic strength. Based on recent studies using photo-inactivation of AMPARs to measure real-time receptor trafficking, it

was proposed that AMPARs from a large internal store exchange rapidly with extrasynaptic somatic AMPARs and subsequently travel to dendrites via lateral diffusion where they are incorporated into synapses (Adesnik et al., 2005). Thus, in the present study, increased SAP97 may "prime" both extrasynaptic and synaptic incorporation of GluR1-containing AMPARs by targeting GluR1 subunits to somatic membranes or by directly driving GluR1 subunit into synapses in response to FZP withdrawal, potentiating glutamatergic synaptic transmission.

Other candidates implicated in "priming" AMPAR trafficking, such as cAMP-dependent protein kinase A (PKA)-mediated phosphorylation, may also be involved and account for the discontinuity between the increase in *sr* GluR1, without a change in *sr* SAP97 levels. It has been reported that direct phosphorylation of GluR1 subunit by PKA permits AMPAR translocation from intracellular pools to the extrasynaptic membrane (Esteban et al., 2003; Oh et al., 2006) and that PKA-mediated phosphorylation may also be associated with GluR1 synaptic remodeling (Oh et al., 2006). Moreover, SAP97 could target A kinase-anchoring protein (AKAP)/PKA complex to GluR1 subunits via a PDZ domain interaction to facilitate phosphorylation of AMPAR GluR1 subunits by PKA (Colledge et al., 2000). Thus, SAP97 and PKA signaling pathways may be cooperatively involved in FZP-withdrawal-induced AMPAR remodeling. Detailed studies on AKAP/PKA complex distribution and activity in response to FZP withdrawal will be helpful. On the other hand, new evidence from our laboratory suggests that CaMKII signaling pathways, linked to LTP induction and maintenance (Soderling and Derkach, 2000) also play a role in enhanced AMPAR function during FZP-withdrawal (Shen and Tietz, 2005, Soc. Neurosci Abstr.).

Another scenario mediating enhanced glutamatergic strength in LTP is an increase in the

proportion of GluR1 subunit-containing synapses. In the adult hippocampus, up to 25% of excitatory synapses do not contain AMPARs and are termed “silent synapses”. Upon LTP induction there is a decrease in the number of synaptic failures, indicating a conversion of silent to non-silent synapses, an effect that depends on increasing synaptic incorporation of GluR1-containing AMPARs (Malinow and Malenka, 2002; Shi et al., 1999). Whether there is a reduction in the proportion of silent synapses in FZP-withdrawn rats remains unclear, and will be resolved with more detailed electrophysiological studies and electron microscopic analysis of the relative distribution of GluR1 and GluR2 subunits in relation to the NMDA receptor NR1 subunit.

Switch in AMPAR composition and its role in FZP withdrawal. Previous studies have indicated that the presence of AMPAR GluR1 subunit alone was sufficient to sustain plasticity, since LTP could still be established in GluR2/3 double knockout mice (Meng et al., 2003). In contrast, a critical role for the AMPAR GluR2 subunit was also found in some studies (Oh and Derkach, 2005). A switch in AMPAR composition has been observed in other forms of plasticity, such as developmental strengthening of excitatory synapses, and after synaptic activation (Liu and Cull-Candy, 2000). Thus, it is important to clarify whether a switch in AMPAR composition is involved in glutamatergic remodeling during FZP withdrawal. Acutely dissociated hippocampal neurons, most but not all with a pyramidal shape, were previously classified into three types: Type I (RI ≈ 1.61, 20.5%), outward rectifying; Type II (RI ≈ 0.5, 23%), inwardly rectifying; Type III (RI ≈ 1.13, 56.4%), linear I-V relationship. The degree of kainate-induced AMPAR-mediated current rectification and Ca^{2+} permeability was inversely correlated (Lerma et al., 1994). The distribution of rectification indices in control pyramidal neurons in the present study is consistent with that

found by Lerma and colleagues. The degree of rectification in CA1 neurons from FZP-withdrawn rats suggests that there was a relative shift in composition of the AMPAR subunit population: more GluR2-lacking AMPARs, possibly GluR1 homomers, were inserted into the membrane, resulting in AMPAR current potentiation. It appears that the removal of membrane-associated GluR2 subunits was not responsible for the shift in rectification, as there was no evidence of an alteration GluR2 subunit expression at any level examined. Meanwhile, surface GluR1 signal and GluR1/2 co-localization were significantly increased in the *sp* and *sr* area during FZP withdrawal. These findings suggest increased delivery of GluR1 homomers to the membrane and also a possible switch in AMPAR composition from GluR2/3 to GluR1/2 heteromers. Immunofluorescence analyses revealed a detectable increase in GluR1 subunit expression in apical (*sr*) dendritic areas, rather than in basal dendrites (*so*). Further electron microscopic studies focusing on GluR1 expression in apical and basal dendritic regions, as well as the relative proportion of GluR1 and GluR2 or GluR3 subunits will be beneficial to further elucidate changes in the synaptic composition of AMPARs during benzodiazepine withdrawal.

Increased glutamatergic strength as a basis for addictive and abusive behaviors. Our studies suggest that an LTP-like increase in glutamatergic strength contributes to CA1 hyperexcitability during benzodiazepine withdrawal; however, the stimulus for membrane delivery of GluR1 subunits remains uncertain. The GABA-mediated depolarization observed in FZP-withdrawn rats (Zeng et al., 1995) might provide the Ca^{2+} influx required to initiate AMPA receptor membrane insertion (Malinow and Malenka, 2002; Oh and Derkach, 2005) via voltage-gated Ca^{2+} channels (Xiang and Tietz, 2007). Moreover, theta activity increases during

FZP withdrawal, consistent with an essential role for septo-hippocampal theta activity in the expression of withdrawal-anxiety (McNaughton and Gray, 2000). Drug-induced enhancement of CA1 neuron output through increased theta activity may provide the neurophysiological basis for contextual memories associated with drug-related environmental cues, implicated in re-instatement of drug-seeking behavior (Nestler, 2005). Thus, overactivation of hippocampal glutamatergic efferent circuits may provide a substrate for the reinforcement of addictive and abusive behaviors elicited by a variety of drugs of abuse, despite diverse pharmacologic sites of action (Malinow and Malenka, 2002; Nestler, 2005). Understanding the role of enhanced glutamatergic function in withdrawal-anxiety is clinically significant, as these symptoms can lead to overuse of benzodiazepines prescribed for anxiety and insomnia, a rising form of prescription drug misuse, and may also be a factor in the increase in benzodiazepine abuse among polydrug abusers (Griffiths and Johnson, 2005).

The finding that FZP withdrawal facilitates extrasynaptic and synaptic AMPAR functions and promotes membrane and synapse targeting of GluR1-containing AMPARs in CA1 pyramidal neurons is novel, and similar to the central mechanism underlying LTP. SAP97 may prime GluR1 subunit redistribution from the cytosol to the plasma membrane, leading to AMPAR current potentiation. Increased membrane incorporation of GluR1 AMPARs, and the consequent potentiation of AMPAR function, may represent a common regulatory mechanism for synaptic remodeling and neuronal signal processing associated with a variety of adaptive behaviors including drug dependence, learning and memory.

Acknowledgements: We are grateful to Francisco J. Alvarez, Bradley J. Van Sickle, Scott Lilly and Paromita Das for critical reading of the manuscript. We thank Kun Xiang for helpful discussions as well as technical assistance. We also acknowledge expert technical assistance from Margarete Otting, Krista Pettee, William J. Ferencak III, and Eugene Orlowski. The National Institute of Drug Abuse Drug Supply Program supplied flurazepam.

References

Adesnik H, Nicoll RA, and England P (2005) Photoinactivation of native AMPA receptors reveals their real-time trafficking. *Neuron* **48**: 977-985.

Bateson AN (2002) Basic pharmacologic mechanisms involved in benzodiazepine tolerance and withdrawal. *Curr Pharm Des* **8**: 5-21.

Borgdorff A and Choquet D (2002) Regulation of AMPA receptor lateral movements. *Nature* **417**: 649-653.

Colledge M, Dean RA, Scott GK, Langeberg LK, Huganir RL, and Scott JD (2000) Targeting of PKA to glutamate receptors through a MAGUK-AKAP complex. *Neuron* **27**: 107-119.

Chouinard G (2004) Issues in the clinical use of benzodiazepines: potency, withdrawal, and rebound. *J Clin Psychiatry* **65** Suppl 5: 7-12.

Downing S, Lee Y, Farb D, and Gibbs T (2005) Benzodiazepine modulation of partial agonist efficacy and spontaneously active GABA(A) receptors supports an allosteric model of modulation. *Br J Pharmacol* **145**: 894-906.

Esteban J, Shi S, Wilson C, Nuriya M, Huganir RL, and Malinow R (2003) PKA phosphorylation of AMPA receptor subunits controls synaptic trafficking underlying plasticity. *Nat Neurosci* **6**: 136-143.

Griffiths R and Johnson MW (2005) Relative abuse liability of hypnotic drugs: a conceptual framework and algorithm for differentiating among compounds. *J Clin Psychiatry* **66** Suppl 9: 31-41.

Izzo E, Auta J, Impagnatiello F, Pesold C, Guidotti A, and Costa E (2001) Glutamic acid

decarboxylase and glutamate receptor changes during tolerance and dependence to benzodiazepines. *Proc Natl Acad Sci U S A* **98**: 3483-3488.

Leonard A, Davare MA, Horne MC, Garner CC, and Hell J (1998) SAP97 is associated with the alpha-amino-3-hydroxy-5-methylisoxazole-4-propionic acid receptor GluR1 subunit. *J Biol Chem* **273**: 19518-19524.

Lerma J, Morales M, Ibarz JM, and Somohano F (1994) Rectification properties and Ca2+ permeability of glutamate receptor channels in hippocampal cells. *Eur J Neurosci* **6**: 1080-1088.

Liu S and Cull-Candy SG (2000) Synaptic activity at calcium-permeable AMPA receptors induces a switch in receptor subtype. *Nature* **405**: 454-458.

Malinow R and Malenka RC (2002) AMPA receptor trafficking and synaptic plasticity. *Annu Rev Neurosci* **25**: 103-126.

Mcnaughton N and Gray J (2000) Anxiolytic action on the behavioural inhibition system implies multiple types of arousal contribute to anxiety. *J Affect Disord* **61**: 161-176.

Meng Y, Zhang Y, and Jia Z (2003) Synaptic transmission and plasticity in the absence of AMPA glutamate receptor GluR2 and GluR3. *Neuron* **39**: 163-176.

Nestler EJ (2005) Is there a common molecular pathway for addiction? *Nat Neurosci* **8**: 1445-1449.

Oh M and Derkach V (2005) Dominant role of the GluR2 subunit in regulation of AMPA receptors by CaMKII. *Nat Neurosci* **8**: 853-854.

Oh M, Derkach VA, Guire ES, and Soderling T (2006) Extrasynaptic membrane trafficking

regulated by GluR1 serine 845 phosphorylation primes AMPA receptors for long-term potentiation. *J Biol Chem* **281**: 752-758.

Partin K, Fleck MW, and Mayer ML (1996) AMPA receptor flip/flop mutants affecting deactivation, desensitization, and modulation by cyclothiazide, aniracetam, and thiocyanate. *J Neurosci* **16**: 6634-6647.

Patneau DK and Mayer ML (1991) Kinetic analysis of interactions between kainate and AMPA: evidence for activation of a single receptor in mouse hippocampal neurons. *Neuron* **6**: 785-798.

Rammes G, Zeilhofer H, Collingridge GL, Parsons C, and Swandulla D (1999) Expression of early hippocampal CA1 LTP does not lead to changes in AMPA-EPSC kinetics or sensitivity to cyclothiazide. *Pflugers Arch* **437**: 191-196.

Sans N, Racca C, Petralia R, Wang Y, Mccallum J, and Wenthold R (2001) Synapse-associated protein 97 selectively associates with a subset of AMPA receptors early in their biosynthetic pathway. *J Neurosci* **21**: 7506-7516.

Seifert G, Zhou M, Dietrich D, Schumacher T, Dybek A, Weiser T, Wienrich M, Wilhelm D, and Steinhauser C (2000) Developmental regulation of AMPA-receptor properties in CA1 pyramidal neurons of rat hippocampus. *Neuropharmacology* **39**: 931-942.

Shi S, Hayashi Y, Esteban J, and Malinow R (2001) Subunit-specific rules governing AMPA receptor trafficking to synapses in hippocampal pyramidal neurons. *Cell* **105**: 331-343.

Shi S, Hayashi Y, Petralia R, Zaman SH, Wenthold R, Svoboda K, and Malinow R (1999) Rapid spine delivery and redistribution of AMPA receptors after synaptic NMDA receptor activation. *Science* **284**: 1811-1816.

Smith KE, Gibson ES, and Dell'Acqua ML (2006) cAMP-dependent protein kinase postsynaptic localization regulated by NMDA receptor activation through translocation of an A-kinase anchoring scaffold protein. *J Neurosci* **26**: 2391-2402.

Soderling T and Derkach V (2000) Postsynaptic protein phosphorylation and LTP. *Trends Neurosci* **23**: 75-80.

Stromgaard K and Mellor I (2004) AMPA receptor ligands: synthetic and pharmacological studies of polyamines and polyamine toxins. *Med Res Rev* **24**: 589-620.

Tietz EI, Zeng X, Chen S, Lilly SM, Rosenberg H, and Kometiani P (1999a) Antagonist-induced reversal of functional and structural measures of hippocampal benzodiazepine tolerance. *J Pharmacol Exp Ther* **291**: 932-942.

Tietz EI, Kapur J, and Macdonald R (1999b) Functional GABAA receptor heterogeneity of acutely dissociated hippocampal CA1 pyramidal cells. *J Neurophysiol* **81**: 1575-1586.

Van Sickle B and Tietz E (2002) Selective enhancement of AMPA receptor-mediated function in hippocampal CA1 neurons from chronic benzodiazepine-treated rats. *Neuropharmacology* **43**: 11-27.

Van Sickle BJ, Xiang K, and Tietz E (2004) Transient Plasticity of Hippocampal CA1 Neuron Glutamate Receptors Contributes to Benzodiazepine Withdrawal-Anxiety. Neuropsychopharmacology **29**: 1994-2006.

Washburn M, Numberger M, Zhang S, and Dingledine R (1997) Differential dependence on GluR2 expression of three characteristic features of AMPA receptors. *J Neurosci* **17**: 9393-9406.

Wenthold R, Petralia R, Blahos JII, and Niedzielski A (1996) Evidence for multiple AMPA receptor complexes in hippocampal CA1/CA2 neurons. *J Neurosci* **16**: 1982-1989.

Wu H, Nash JE, Zamorano P, and Garner CC (2002) Interaction of SAP97 with minus-end-directed actin motor myosin VI: Implications for AMPA receptor trafficking. *J Biol Chem* **277**: 30928-30934.

Xiang K and Tietz EI (2007) Benzodiazepine-induced hippocampal CA1 neuron AMPA receptor plasticity linked to severity of withdrawal-anxiety: Differential role of voltage-gated calcium channels and NMDA receptors. *Behav Pharmacol* (Special Issue: The Behavioral Pharmacology of the Hippocampus), in press.

Xie X and Tietz E (1992) Reduction in potency of selective gamma-aminobutyric acidA agonists and diazepam in CA1 region of in vitro hippocampal slices from chronic flurazepam-treated rats. *J Pharmacol Exp Ther* **262**: 204-211.

Zamanillo D, Sprengel R, Hvalby O, Jensen V, Burnashev N, Rozov A, Kaiser KM, Koster H, Borchardt T, Worley P, Lubke J, Frotscher M, Kelly P, Sommer B, Andersen P, Seeburg P, and Sakmann B (1999) Importance of AMPA receptors for hippocampal synaptic plasticity but not for spatial learning. *Science* **284**: 1805-1811.

Zeng X, Xie XH, and Tietz EI (1995) Reduction of GABA-mediated inhibitory postsynaptic potentials in hippocampal CA1 pyramidal neurons following oral flurazepam administration. *Neuroscience* **66**: 87-99.

Zeng X and Tietz EI (1999) Benzodiazepine tolerance at GABAergic synapses on hippocampal CA1 pyramidal cells. *Synapse* **31**: 263-277.

Footnotes: This work was supported by Department of Health and Human Services grants from the National Institute on Drug Abuse: R01-DA-04075-15 and R01-DA18342-02 to EIT; and predoctoral fellowships from the University of Toledo College of Medicine to JS and GS.

Legends for Figures

Figure 1. AMPAR current density is increased in dissociated CA1 neurons after FZP withdrawal. Currents were recorded at V_H = -60 mV with 0.5 μM TTX, 200 μM $CdCl_2$ and 100 μM APV in isolated neurons from control (CON) and 2-day FZP-withdrawn (FZP) rats. (**A**) Photomicrograph of an acutely dissociated neuron. Scale bar: 40 μm. (**B**) Evoked AMPAR-mediated currents after ultra-rapid, 1 mS application of 2 mM glutamate (Glu). (**C**) Glutamate-induced current density (pA/pF) was significantly increased after 2-day FZP withdrawal (n = 21 cells/6 rats per group). (**D**) Currents evoked by the AMPAR agonist kainate (KA, 300 μM) during a 1mV/ms voltage ramp as shown in Figure 2E. KA-induced current density (pA/pF) at V_H = -60 mV was significantly increased after 2-day FZP withdrawal (CON: n = 14 cells/3 rats; FZP: n = 21 cells/3 rats, $p < 0.02$). (**E**) Currents evoked by 180 ms application of 2 mM glutamate. (**F**) No significant difference in tau of desensitization between CON and FZP groups (CON: n = 15 cells/5 rats; FZP: n = 16 cells/5 rats). (**G**) Representative currents elicited by a 10 ms application of increasing glutamate concentrations (30 μM to 3000 μM). (**H**) Concentration-response curve representing average AMPAR current density (CON: solid circles; FZP: open circles). Current densities (pA/pF) were significantly increased in the FZP group at glutamate concentrations from 500 μM to 3000 μM (CON: n = 10 cells/7 rats; FZP: n = 13 cells/7 rats). Data are represented by mean ± SEM; Error bars in this and all other figures represent the SEM. Asterisks: $p < 0.05$ by unpaired Student's *t*-test.

JPET Fast Forward. Published on May 17, 2007 as DOI: 10.1124/jpet.107.121798
This article has not been copyedited and formatted. The final version may differ from this version.

Figure 2. Shift towards inward rectification and spermine blockade of agonist-evoked currents in CA1 neurons after FZP withdrawal. (**A**) AMPAR-mediated currents were recorded at -60 and +40 mV holding potentials in isolated neurons after 1 ms application of 2 mM glutamate with 0.5 μM TTX, 200 μM $CdCl_2$ and 100 μM APV in the bath. Spermine (100 μM) was included in the micropipette to replace endogenous spermine lost during dialysis. (**B**) The rectification index (+40/-60 mV) for glutamate was significantly decreased after 2-day FZP withdrawal (CON: 18 cells/ 6 rats; FZP: 20 cells/6 rats). (**C**) Representative averaged AMPAR-mediated mEPSCs recorded at -60 and +40 mV holding potentials in hippocampal slices in the presence of 1 μM TTX, 50 μM APV, and 50 μM picrotoxin, 25 μM CGP35348 and with spermine in the micropipette. (**D**) The mEPSC rectification index (+40/-60 mV) was significantly decreased after 2-day FZP withdrawal (CON: 9 cells/8 rats; FZP: 11 cells/6 rats). Asterisk in B and D: $p < 0.05$ by unpaired Student's *t*-test. (**E**) Representative pair of voltage-ramps at holding potentials from -100 to +80 mV generated at 1 mV/ms during 300 μM KA application. The current density from the FZP neuron was normalized to the CON neuron. At positive holding potentials, the CON neuron showed outward rectification (slope ratio = 1.46), while the FZP neuron rectification was nearly linear (slope ratio = 1.08). (**F**) The distribution of slope ratios from individual CON (closed circles) and FZP neurons (open circles). The slope ratios (+35 to +45 mV/-65 to -55 mV) derived from the voltage ramp during KA application were significantly decreased after 2-day FZP withdrawal (CON: 14 cells/3 rats; FZP: 21 cells/3 rats). Horizontal bar represents the mean. Asterisks: $p < 0.001$ by unpaired Student's *t*-test. (**G**) Representative currents elicited at -80 mV by 6 s 300 μM KA and 2 s co-application of 100 μM NAS without intracellular spermine. (**H**) Cells from the FZP

group exhibited significantly increased NAS blockade compared to the CON group, (CON: 16 cells/3 rats; FZP: 13 cells/3 rats). Asterisks: $p < 0.001$ by Mann-Whitney U test.

Figure 3. Surface GluR1, but not GluR2, subunit immunofluorescence is increased in CA1 neurons after FZP withdrawal. GluR1 and GluR2 surface expression were detected with anti-N-terminal antibodies. (**A**) Surface GluR1 subunit staining in hippocampal CA1 area (*so*: stratum oriens; *sp*: stratum pyramidale; *sr*: stratum radiatum). Scale bar: 50 μm. (**B**) Gamma globulin controls for surface GluR1 (middle) and GluR2 (right). Scale bar: 20 μm. (**C**) Representative photomicrographs of GluR1 (left), GluR2 (middle) and colocalization of GluR1/2 staining (right) in *sp* from the CON (upper panels) and FZP (lower panels) groups. Scale bar: 20 μm. Arrows within inset images (enlarged 200%) depict examples of co-localized signal at the membrane, quantified in E as a function of cell circumference. (**D**) Representative photomicrographs of GluR1 (left), GluR2 (middle) and colocalization of GluR1/2 staining (right) in the first 100 μm of the apical dendritic area (*sr*) immediately adjacent to *sp*, from the CON (upper panels) and FZP (lower panels) groups, Scale bar: 20 μm. (**E**) Quantification of GluR1 (left), GluR2 (middle) and colocalization of GluR1/2 (right) immunofluorescence signals in *sp*. The FZP group showed a significant increase in surface GluR1 signal (mean density) compared with the CON group by Mann-Whitney U Test. No significant differences were found in GluR2 signal between groups. Quantification of GluR1/2 colocalization signal between groups showed a significant increase in particle mean signal density and particle number/cell in the FZP group by unpaired Student's *t* test. (**F**) Quantification of GluR1 (left), GluR2 (middle) and colocalization of

GluR1/2 (right) immunofluorescence signal in *sr*. The FZP group showed a significant increase in surface GluR1 signal (mean density) by unpaired Student's *t* test. No significant differences were found in GluR2 signal between groups. Quantification of GluR1/2 colocalization signal between groups showed a significant increase in particle mean signal density and particle number/dendrite length by unpaired Student's *t* test. CON: n = 19-27 cells/4 rats; FZP: n = 19-28 cells/4 rats. Asterisk: $p < 0.05$; double asterisks: $p < 0.01$; and triple asterisks: $p < 0.001$.

Figure 4. PSD-95 distribution in subcellular compartments from CA1 miniclices. The PSD-95 signal was enriched in the P3, as compared to the crude membrane (P2) fraction. The density ratio of PSD-95/actin was 1.35 in P2 and 1.92 in P3. The signal ratio was negligible in S2 (0.03) and S3 (0.07) fractions.

Figure 5. Total GluR1, rather than GluR2, protein levels were enhanced in CA1 neurons after FZP withdrawal. CA1 minislices from pairs of control (CON) and FZP-withdrawn groups were fractionated to obtain S2 (cytosolic), P2 (crude membrane) and P3 (PSD-enriched) fractions. GluR1 and GluR2 signal densities were normalized to the respective actin signal. (**A**) Total GluR1 signal density was significantly increased in S2, P2 and P3 fractions derived from of FZP-withdrawn rats. Representative blots are illustrated in the top panel; quantitative analyses of signal density are shown in the histograms below (single asterisk: $p < 0.05$, n = 7/group). GluR1 subunit protein did not redistribute during 2-day FZP withdrawal with P2/S2 ratio 105 ± 17% of control ($p > 0.05$). S2 and P2: 15 μg protein/well; P3: 10 μg protein/well. (**B**) GluR2 signal density

did not change in any fraction in response to FZP withdrawal ($p > 0.05$, n = 7/group). Although there was a slight increase in GluR2 P2/S2 ratio in FZP rats (41 ± 37%), no significant difference was found between groups. All data were analyzed by Student's *t* test. All fractions loaded with 15 μg protein/well.

Figure 6. SAP97 signal increased in CA1 neurons after FZP withdrawal. SAP97 immunoreactivity was detected with confocol imaging (**A**) and immunoblotting (**B**). (**A**) Representative images of SAP97 signal from control (CON) and FZP-withdrawn groups (*sp*: upper panels; *sr*: lower panels). Scale bar: 50 μm or 20 μm for *sp* or *sr*, respectively. Quantifications of SAP97 signal is shown in the panel at right. Compared with the CON group, the FZP group showed a significant increase in *sp* SAP97 signal (mean density) by Mann-Whitney U Test. No significant differences in *sr* SAP97 signal were found between groups. CON and FZP: n = 19 cells/4 rats per group. Single asterisk: $p < 0.05$. (**B**) SAP97 signal density was normalized to the respective actin signal. There were significant increases in SAP97 signal density in the crude membrane (P2) and PSD-enriched (P3) fractions from CA1 minislices of FZP-withdrawn rats compared to the CON group. Representative immunoblots are illustrated in the top panel; quantitative analyses of signal density is shown in the histograms below. Redistribution of SAP97 was also observed in the FZP-withdrawn group with a P2/S2 ratio 144 ± 15% of the CON group. Single asterisk: $p < 0.05$, n = 6-7 pairs of rats. P3 SAP97 signal was analyzed by Mann-Whitney U Test; other fractions were analyzed by Student's *t* test. S2 and P2: 15 μg protein/well; P3: 10 μg protein/well.

JPET Fast Forward. Published on May 17, 2007 as DOI: 10.1124/jpet.107.121798
This article has not been copyedited and formatted. The final version may differ from this version.

Tables

Table 1. AMPAR kinetics of 1 ms glutamate (2 mM) application. Whole-cell recordings were made on lifted CA1 pyramidal neurons with ultra-fast drug application system. Current density was significantly increased during FZP withdrawal in the absence of alterations of AMAPR channel kinetics. C_m: membrane capacitance; R_a: access resistance; Rise time: 10-90% rise time; I_{peak}: peak amplitude of current. Data were listed as mean ± SEM (number of cells). C_m, R_a, I_{peak} and current density were analyzed by two-tailed unpaired Student's *t* test; 10-90% rise time and decay time were analyzed by Mann-Whitney U test. Single asterisk indicates a significant difference ($p < 0.05$).

GROUP	C_m (pF)	R_a (MOhm)	Rise time† (ms)	I_{peak} (pA)	Current density (pA/pF)	Decay time (ms)
CON	20.8 ± 0.6 (18)	15.0 ± 0.9 (18)	1.3 ± 0.1 (18)	4185.4 ± 479.0 (18)	200.0 ± 21.5 (18)	16.2 ± 1.1 (18)
FZP	19.6 ± 0.5 (19)	13.4 ± 0.7 (19)	1.3 ± 0.1 (19)	5248.6 ± 482.2 (19)	268.8 ± 22.8 (19)*	17.3 ± 1.0 (19)

JPET Fast Forward. Published on May 17, 2007 as DOI: 10.1124/jpet.107.121798
This article has not been copyedited and formatted. The final version may differ from this version.

Table 2. Characteristics of mEPSCs. Miniature EPSCs were recorded in CA1 pyramidal neurons in hippocampal slices at V_H = -60 mV and +40 mV. There was a significant increase in mEPSC peak current amplitude in FZP-withdrawn neurons at V_H = -60 mV. RMP: resting membrane potential. Peak current amplitude (I_{peak}) was derived from the averaged events with a rise time < 5 ms. Data listed as mean ± SEM (number of cells) were analyzed by two-tailed unpaired Student's *t* test. Single asterisk indicates a statistically significant difference ($p < 0.05$).

GROUP	RMP (mV)	V_H = -60 mV			V_H = +40 mV		
		I_{peak} (pA)	Rise time (ms)	Decay (τ, ms)	I_{peak} (pA)	Rise time (ms)	Decay (τ, ms)
CON	67.3 ± 0.8 (9)	7.0 ± 0.3 (9)	2.8 ± 0.2 (9)	15.0 ± 1.0 (9)	5.3 ± 0.2 (9)	3.4 ± 0.4 (9)	12.5 ± 3.0 (9)
FZP	64.8 ± 1.3 (11)	8.3 ± 0.3 (11)*	2.7 ± 0.1 (11)	16.0.± 1.1 (11)	4.9 ± 0.3 (11)	2.9 ± 0.2 (11)	14.1 ± 3.5 (11)

JPET Fast Forward. Published on May 17, 2007 as DOI: 10.1124/jpet.107.121798
This article has not been copyedited and formatted. The final version may differ from this version.

Figure 1

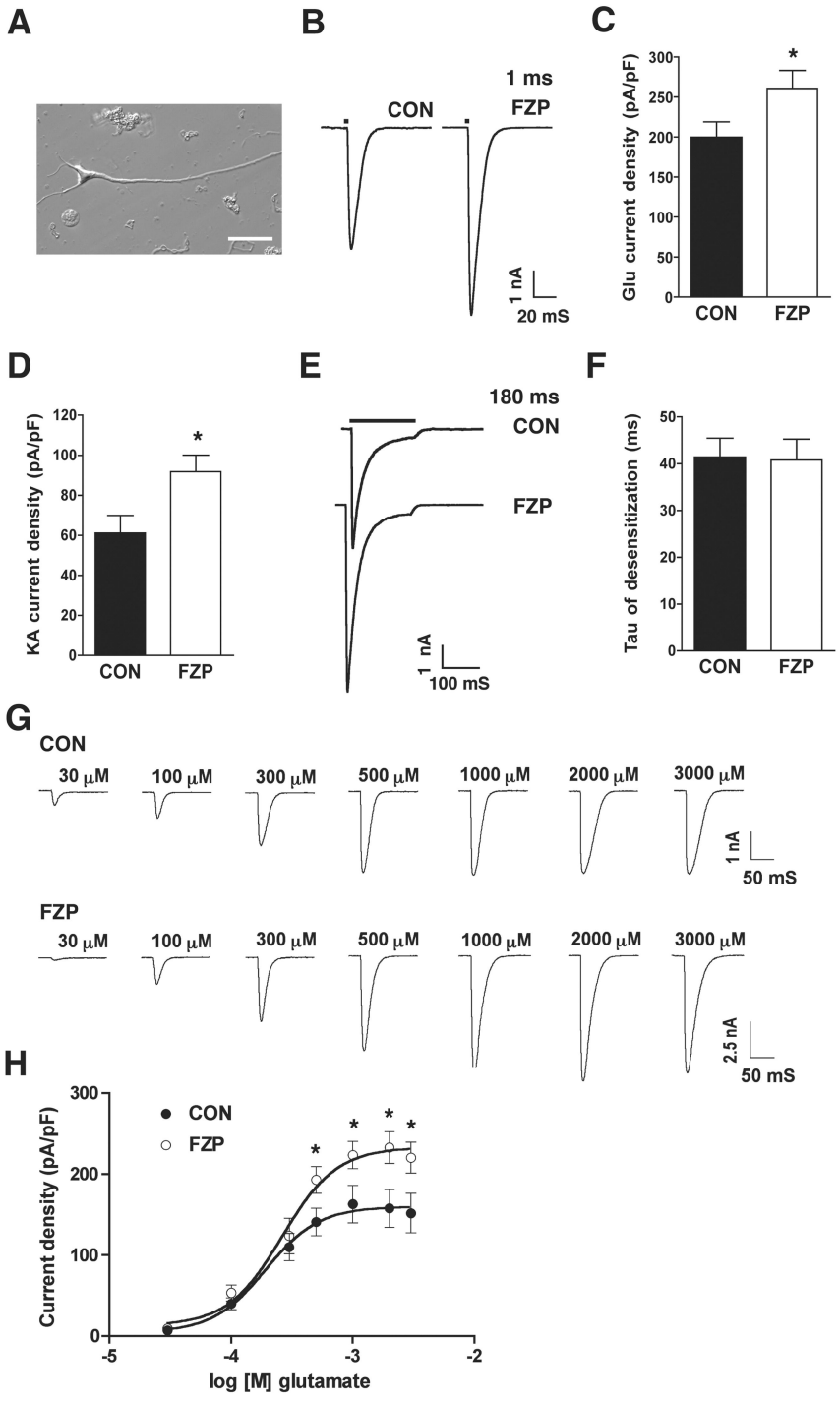

JPET Fast Forward. Published on May 17, 2007 as DOI: 10.1124/jpet.107.121798
This article has not been copyedited and formatted. The final version may differ from this version.

Figure 2

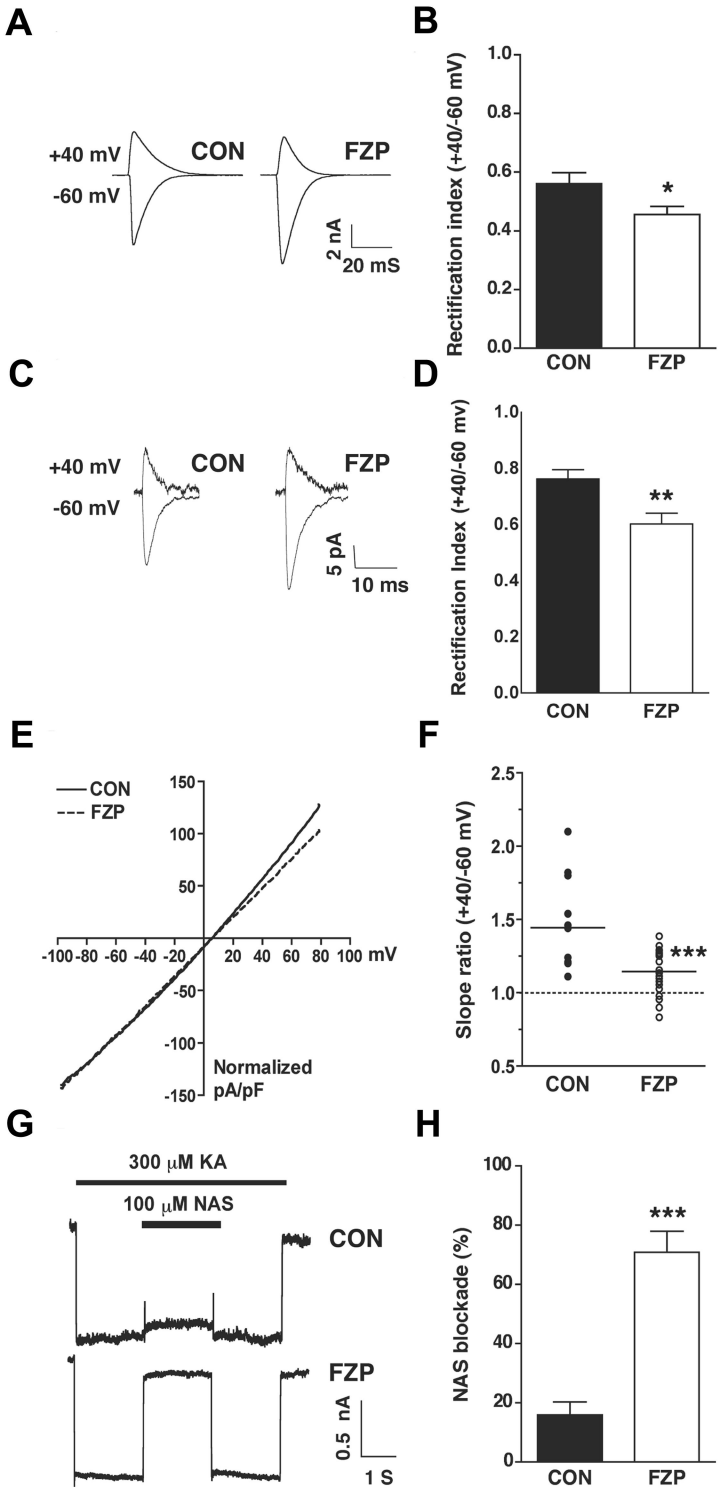

JPET Fast Forward. Published on May 17, 2007 as DOI: 10.1124/jpet.107.121798
This article has not been copyedited and formatted. The final version may differ from this version.

Figure 3

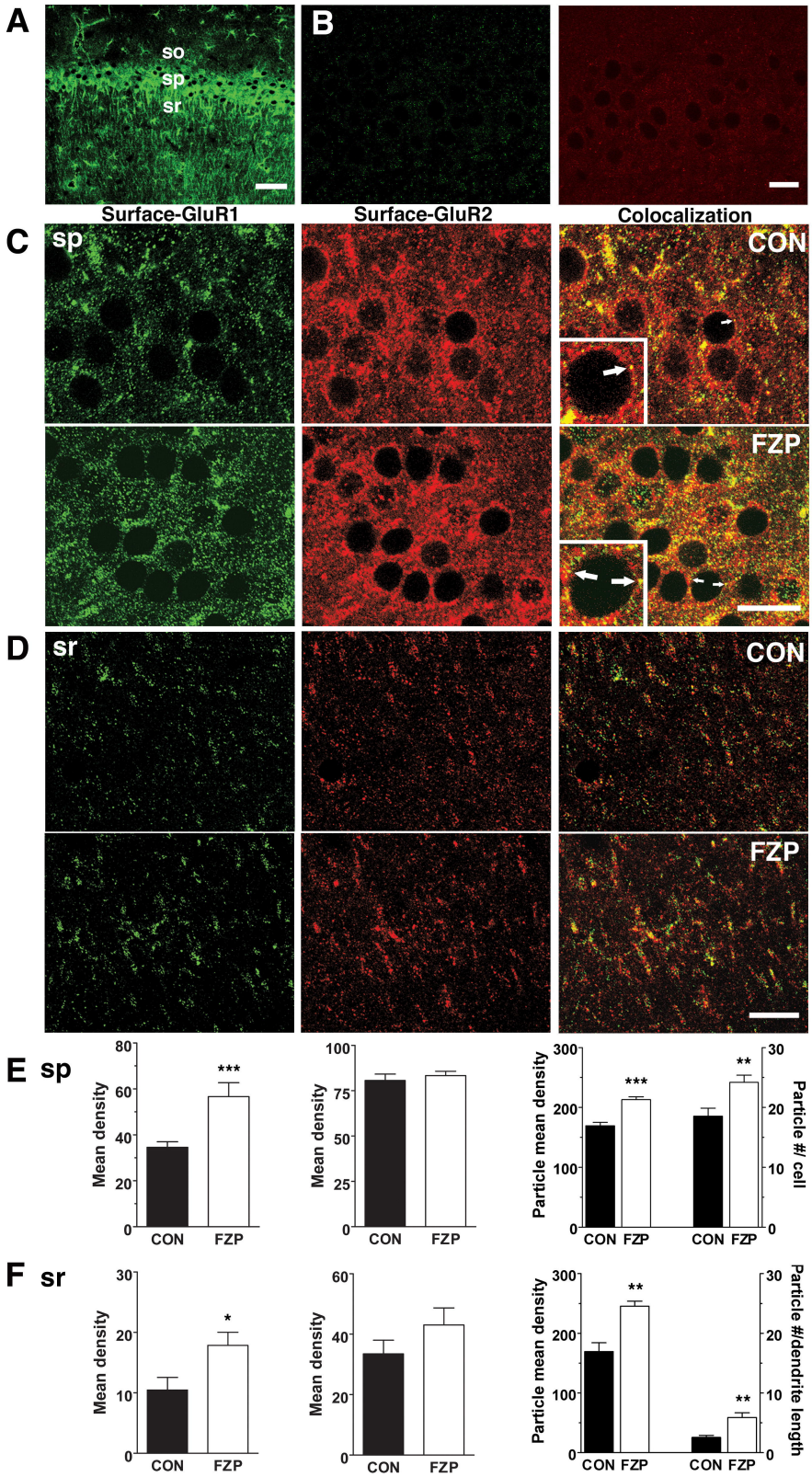

JPET Fast Forward. Published on May 17, 2007 as DOI: 10.1124/jpet.107.121798
This article has not been copyedited and formatted. The final version may differ from this version.

Figure 4

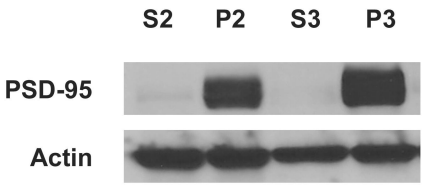

JPET Fast Forward. Published on May 17, 2007 as DOI: 10.1124/jpet.107.121798
This article has not been copyedited and formatted. The final version may differ from this version.

Figure 5

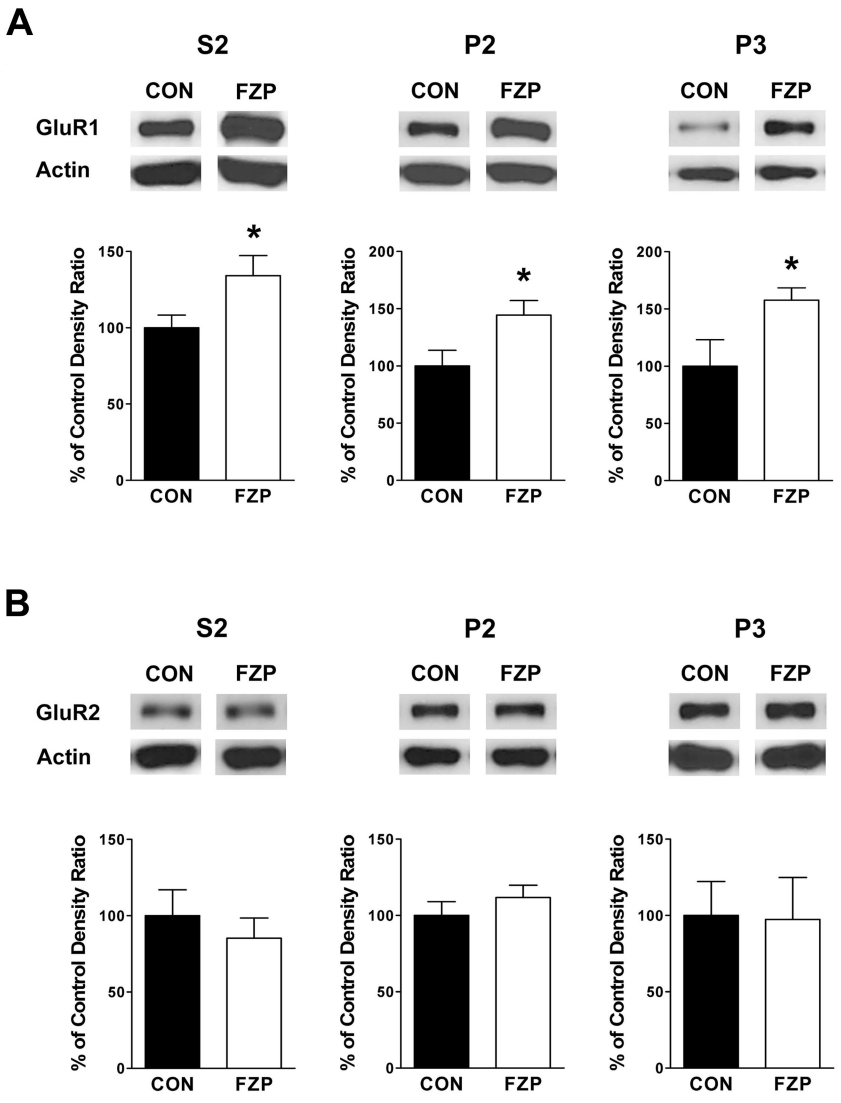

JPET Fast Forward. Published on May 17, 2007 as DOI: 10.1124/jpet.107.121798
This article has not been copyedited and formatted. The final version may differ from this version.

Figure 6